Bistable behavior of pump, probe, and conjugate signals through collinear intracavity nearly degenerate four-wave mixing

N. C. Kothari and R. Frey
Laboratoire d'Optique Quantique du Centre National de la Recherche Scientifique, Ecole Polytechnique, 91128 Palaiseau Cédex, France
(Received 24 January 1986)

Theoretical calculations regarding the collinear intracavity nearly degenerate four-wave mixing are presented when a Fabry-Perot cavity is externally driven by a strong pump and probed by a weak signal. The calculations are performed for two different limits: the mean-field and the small-signal gain approximations. The results suggest the bistable behavior for all the three signals (pump, probe, and conjugate) with several different shapes of the hysteresis loops. Furthermore, for certain values of the parameters in the mean-field approximation, calculations show a resonance behavior of probe and conjugate signals with respect to the incident pump intensity, with probe and conjugate transmittance as high as 10^3–10^4 in the case when the pump transmission does not exhibit bistability. In the small-signal gain approximation, theory also demonstrates strong dependence of probe amplification on the normalized detuning when it is smaller than the probe-cavity mistuning.

I. INTRODUCTION

The geometry of two counterpropagating optical beams of the same frequency interacting in a nonlinear medium is of great importance in nonlinear optics, and has been used to explain several interesting phenomena such as optical bistability,[1] phase conjugation through degenerate four-wave mixing[2] (DFWM) and nearly degenerate four-wave mixing (NDFWM), periodic and chaotic self-pulsations,[3] and so on. Phase conjugation through DFWM has found applications in various fields[4] such as real-time holography, adaptive optics, and laser resonators, and NDFWM can be used to construct a narrow optical bandpass filter with very high Q and four-wave parametric oscillators.[5] DFWM and NDFWM can be achieved in resonant absorbing systems[5,6] as well as in saturable amplifiers,[7,8] with the advantage of obtaining much higher conjugate reflectivities[8] in amplifiers even with low-intensity incident pump beams. In almost all DFWM and NDFWM experiments, the conjugate and pump beams are separated from each other by a noncollinear geometry.[5–7] However, higher conversion efficiencies can be achieved by using a collinear interaction,[8–10] since the interaction can take place along the whole length of the nonlinear material. The beam separation in collinear geometry for DFWM can be obtained by selecting different polarizations for pump and probe beams,[10] whereas in the case of NDFWM it is achieved automatically[8] since pump and probe beams have slightly different frequencies ω and $\omega-\delta\omega$, respectively, with the conjugate beam generated at frequency $\omega+\delta\omega$. Recently, Nakajima and Frey[8] have demonstrated collinear intracavity NDFWM in a $Ga_xAl_{1-x}As$ semiconductor laser oscillator, where they obtained conjugate reflectivities as high as 5000 with a high conversion efficiency of about 25%. Theoretical calculations based on a two-level system explain their experimental results.[11]

When an externally driven nonlinear Fabry-Perot interferometer with bistable transmission is probed[12] through a weak optical field, the nonlinear interaction among the counterpropagating pump beams and the probe generates the phase-conjugated beam in the noncollinear geometry through intracavity DFWM, where the conjugated reflectivity also displays the bistability and hysteresis as the driving field is varied in a continuous manner. The direct observations of bistable behavior of all the three signals (pump, probe, and conjugate) have been recently reported using atomic sodium vapor[13] and $Ga_xAl_{1-x}As$ semiconductor laser amplifier[14] as the nonlinear media. In Ref. 14 a collinear (on-axis) geometry and NDFWM process were used in the experiments, and conjugated reflectivities larger than 500% with 35% efficiency were reported. In the collinear intracavity NDFWM geometry,[14] the high-intensity pump beam of frequency ω and the low-intensity probe beam of frequency $\omega-\delta\omega$ ($\delta\omega \ll \omega$) are sent copropagating through the nonlinear medium kept inside a Fabry-Perot cavity. The total electric field inside the cavity is composed of forward and backward pump, probe, and conjugate waves at frequencies ω, $\omega-\delta\omega$, and $\omega+\delta\omega$, respectively. There are reflected and transmitted outputs at three frequencies, each of which may be independently analyzed. In this paper, the theory is formulated to explain the bistable behavior of the three signals observed by using this collinear intracavity NDFWM geometry, shown in Fig. 1. The nonlinear response of the two-level system used in this theory is calculated using the density-matrix formalism, and propagation effects are included by solving coupled-wave equations for all six waves. The standing-wave effects arising from interference of the counterpropagating waves are fully incorporated. The propagation equations are, then, solved for two different limits: the mean-field approximation where low absorption and high mirror reflectivities of the Fabry-Perot cavity are assumed, and the small-signal gain approximation

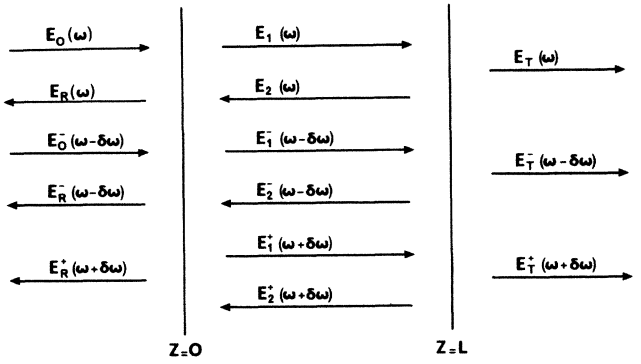

FIG. 1. Geometry for collinear intracavity nearly degenerate four-wave mixing. The Fabry-Perot cavity is externally driven by a strong pump field and probed by a weak field collinearly.

where pump intensities are assumed to be small compared to the saturation intensity of a medium having gain (laser amplifier). In both these cases, the pump depletion is neglected, assuming probe and conjugate signals to be much smaller than the pump.

In Sec. II the expressions for the polarizations at three frequencies ω, $\omega-\delta\omega$, and $\omega+\delta\omega$ are given, and in Sec. III six coupled propagation equations for the six waves (forward and backward pump, probe, and conjugate) are derived. These equations are solved for two cases mentioned above for Fabry-Perot boundary conditions in Secs. IV and V. Finally, Sec. VI is devoted to discussion and conclusions.

II. NONLINEAR RESPONSE OF A TWO-LEVEL SYSTEM

In this section, response of the atoms to a strong pump field at frequency ω and weak probe and conjugate fields at frequencies $\omega-\delta\omega$ and $\omega+\delta\omega$, respectively, is calculated using the density matrix formalism. The equations of motion for the elements ρ_{ij} of the density matrix have the form[15]

$$i\hbar\frac{dN}{dt}=2(\rho_{ba}V_{ab}-V_{ba}\rho_{ab})-i\hbar\frac{N-N_0}{T_1}\ , \tag{1a}$$

$$i\hbar\frac{d\rho_{ab}}{dt}=-\hbar\omega_0\rho_{ab}-V_{ab}N-i\hbar\frac{\rho_{ab}}{T_2}\ , \tag{1b}$$

where a and b denote, respectively, the ground and upper atomic levels separated by energy $\hbar\omega_0$; T_1 and T_2 are longitudinal and transverse relaxation times, respectively; and $N=\rho_{aa}-\rho_{bb}$ is the population difference between the two levels a and b with N_0 denoting the equilibrium population difference in the absence of the optical fields. The matrix elements of the interaction energy V_{ab} $(=V_{ba}^*)$ are given in the rotating-wave approximation by

$$V_{ab}=-\mu_{ab}[E(\omega)e^{-i\omega t}+E^-(\omega-\delta\omega)e^{-i(\omega-\delta\omega)t}+E^+(\omega+\delta\omega)e^{-i(\omega+\delta\omega)t}+\text{c.c.}]\ . \tag{2}$$

Here, μ_{ab} denotes the transition dipole moment. Assuming $|E^{\pm}(\omega\pm\delta\omega)|\ll|E(\omega)|$, steady-state solutions[16] to these equations of motion can be found using perturbation method correct to all orders in the amplitudes of the pump waves at frequency ω and to first order in the amplitudes of the weak fields at $\omega\pm\delta\omega$. Then, the polarizations at three frequencies ω, $\omega\pm\delta\omega$ can be given by the following expressions:

$$P(\omega)=\chi E\ , \tag{3a}$$

$$P(\omega+\delta\omega)=\chi_1E^+ +\chi_3(E^-)^*\ , \tag{3b}$$

and

$$P^*(\omega-\delta\omega)=\chi_3E^+ +\chi_4(E^-)^*\ , \tag{3c}$$

where

$$\chi=\frac{\alpha_0c\eta}{4\pi\omega}\frac{(\Delta+i)}{1+\Delta^2+\left|\frac{E(\omega)}{E_s}\right|^2}\ , \tag{4a}$$

$$\chi_1=\frac{\alpha_0c\eta}{4\pi\omega}\frac{\Delta^-+i}{1+\Delta^{-2}}\left[\frac{(1+\Delta^2)}{1+\Delta^2+\left|\frac{E(\omega)}{E_s}\right|^2}+\frac{C^*}{A^*}\left|\frac{E(\omega)}{E_s}\right|^2\right], \tag{4b}$$

$$\chi_2=\frac{\alpha_0c\eta}{4\pi\omega}\frac{\Delta^-+i}{1+\Delta^{-2}}\frac{B^*}{A^*}\frac{E^2(\omega)}{|E_s|^2}\ , \tag{4c}$$

$$\chi_3=\frac{\alpha_0c\eta}{4\pi\omega}\frac{\Delta^+-i}{1+\Delta^{+2}}\frac{C^*}{A^*}\frac{E^{*2}(\omega)}{|E_s|^2}\ , \tag{4d}$$

and

$$\chi_4=\frac{\alpha_0c\eta}{4\pi\omega}\frac{\Delta^+-i}{1+\Delta^{+2}}\left[\frac{(1+\Delta^2)}{1+\Delta^2+\left|\frac{E(\omega)}{E_s}\right|^2}+\frac{B^*}{A^*}\left|\frac{E(\omega)}{E_s}\right|^2\right], \tag{4e}$$

with

$$A=\delta_1-i+\frac{1}{2}\left[\frac{\Delta^--i}{1+\Delta^{-2}}-\frac{\Delta^++i}{1+\Delta^{+2}}\right]\left|\frac{E(\omega)}{E_s}\right|^2, \tag{5a}$$

$$B=-\frac{1}{2\left[1+\Delta^2+\left|\frac{E(\omega)}{E_s}\right|^2\right]}\times\left[\Delta-i-(\Delta^++i)\frac{1+\Delta^2}{1+\Delta^{+2}}\right], \tag{5b}$$

and

$$C=\frac{1}{2\left[1+\Delta^2+\left|\frac{E(\omega)}{E_s}\right|^2\right]}\times\left[\Delta+i-(\Delta^--i)\frac{1+\Delta^2}{1+\Delta^{-2}}\right]. \tag{5c}$$

The quantities α_0 and $|E_s|^2$ are the resonant absorption coefficient and the saturation intensity of the two-level system, respectively, and they are given by $\alpha_0=(4\pi N_0\mu_{ab}^2\omega T_2)/\hbar c\eta$ and $|E_s|^2=\hbar^2/4\mu_{ab}^2T_1T_2$. In the above expressions, c is the velocity of light in a vacuum, η is the linear refractive index of the medium, $i=\sqrt{-1}$, and $\hbar=h/2\pi$ is Planck's constant. Also, the quantities Δ, Δ^-, Δ^+, and δ_1 are defined by $\Delta=(\omega_0-\omega)T_2$, $\Delta^-=(\omega_0-\omega-\delta\omega)T_2$, $\Delta^+=(\omega_0-\omega+\delta\omega)T_2$, and $\delta_1=\delta\omega T_1$.

III. THE WAVE EQUATIONS WITH THE NONLINEAR POLARIZATION

In this section, propagation effects are considered by treating the nonlinear polarizations as source terms in Maxwell's equations for the three frequencies of interest. Under the assumption of slowly varying envelopes of the fields, the three propagation equations for the waves at three frequencies for the steady-state conditions using paraxial and plane-wave approximations are written as

$$2ik\frac{dA_1}{dz}e^{ikz}-2ik\frac{dA_2}{dz}e^{-ikz}=-\frac{4\pi\omega^2}{c^2}P(\omega), \tag{6a}$$

$$2ik^+\frac{dA_1^+}{dz}e^{ik^+z}-2ik^+\frac{dA_2^+}{dz}e^{ik^+z}=-\frac{4\pi\omega^2}{c^2}P(\omega+\delta\omega), \tag{6b}$$

$$2ik^-\frac{dA_1^-}{dz}e^{ik^-z}-2ik^-\frac{dA_2^-}{dz}e^{ik^-z}=-\frac{4\pi\omega^2}{c^2}P(\omega-\delta\omega), \tag{6c}$$

where the electric field amplitudes at three frequencies are taken as $E(\omega)=A_1e^{ikz}+A_2e^{-ikz}$ and $E^{\pm}(\omega\pm\delta\omega)=A_1^{\pm}e^{ik^{\pm}z}+A_2^{\pm}e^{-ik^{\pm}z}$. The right-hand side of Eqs. (6) have dc spatial components as well as high-frequency spatial components due to the $|E(\omega)/E_s|^2$ term. Only the dc components are phase matched and, hence, of importance in coupled equations. Writing

$$A_1=|A_1|e^{iq_1},\quad A_2=|A_2|e^{iq_2},\quad I_1=\left|\frac{A_1}{E_s}\right|^2,$$

and

$$I_2=\left|\frac{A_2}{E_s}\right|^2,$$

$|E(\omega)/E_s|^2$ is given by

$$\left|\frac{E(\omega)}{E_s}\right|^2=I_1+I_2+2(I_1I_2)^{1/2}\cos\theta, \tag{7}$$

where $\theta=2kz+q_1-q_2$ is the relative phase between the forward and backward pump waves. Expanding $\chi(E)$ and χ_j $(j=1,2,3,4)$ in Eqs. (4) into their Fourier components, and substituting Eqs. (3) into Eqs. (6), one obtains, after equating the coefficients of $e^{\pm ikz}$, $e^{\pm ik^-z}$, $e^{\pm ik^+z}$, the following six equations for the field envelopes $A_i(\omega)$, $A_i^+(\omega+\delta\omega)$, and $A_i^-(\omega-\delta\omega)$ $(i=1,2)$:

$$\frac{dA_1}{dz}=-\frac{\alpha_0}{2}(1-i\Delta)(a_0A_1+e^{i(q_1-q_2)}a_1A_2), \tag{8a}$$

$$\frac{dA_2}{dz}=\frac{\alpha_0}{2}(1-i\Delta)(a_0A_2+e^{-i(q_1-q_2)}a_{-1}A_1), \tag{8b}$$

$$\frac{dA_1^+}{dz}=-\frac{\alpha_0^+}{2}\{b_0A_1^++c_0e^{-i\Delta kz}(A_2^-)^*+e^{i(q_1-q_2)}[c_1(A_1^-)^*+b_1e^{-i\Delta kz}A_2^+]\}, \tag{8c}$$

$$\frac{dA_2^+}{dz}=\frac{\alpha_0^+}{2}\{b_0A_2^++c_0e^{i\Delta kz}(A_1^-)^*+e^{-i(q_1-q_2)}[c_{-1}(A_2^-)^*+b_{-1}e^{i\Delta kz}A_1^+]\}, \tag{8d}$$

$$\frac{d(A_1^-)^*}{dz}=-\frac{\alpha_0^-}{2}\{e_0(A_1^-)^*+d_0e^{-i\Delta kz}A_2^++e^{-i(q_1-q_2)}[d_{-1}A_1^++e_{-1}e^{-i\Delta kz}(A_2^-)^*]\}, \tag{8e}$$

$$\frac{d(A_2^-)^*}{dz}=\frac{\alpha_0^-}{2}\{e_0(A_2^-)^*+d_0e^{i\Delta kz}A_1^++e^{i(q_1-q_2)}[d_1A_2^++e_1e^{i\Delta kz}(A_1^-)^*]\}, \tag{8f}$$

where

$$a_n=\frac{4\pi\omega}{(\Delta+i)\alpha_0c\eta}\frac{1}{2\pi}\int_{-\pi}^{\pi}\chi(\theta)e^{-in\theta}d\theta, \tag{9a}$$

$$b_n=\frac{4\pi\omega}{\alpha_0c\eta}\frac{1+\Delta^{-2}}{\Delta^-+i}\frac{1}{2\pi}\int_{-\pi}^{\pi}\chi_1(\theta)e^{-in\theta}d\theta, \tag{9b}$$

$$c_n=\frac{4\pi\omega}{\alpha_0c\eta}\frac{1+\Delta^{-2}}{\Delta^-+i}\frac{1}{2\pi}\int_{-\pi}^{\pi}\chi_2(\theta)e^{-in\theta}d\theta, \tag{9c}$$

$$d_n=\frac{4\pi\omega}{\alpha_0 c\eta}\frac{1+\Delta^{+2}}{\Delta^+-i}\frac{1}{2\pi}\int_{-\pi}^{\pi}\chi_3(\theta)e^{-in\theta}d\theta\,, \tag{9d}$$

$$e_n=\frac{4\pi\omega}{\alpha_0 c\eta}\frac{1+\Delta^{+2}}{\Delta^+-i}\frac{1}{2\pi}\int_{-\pi}^{\pi}\chi_4(\theta)e^{-in\theta}d\theta\,. \tag{9e}$$

In these expressions $\alpha_0^+=\alpha_0/(1+i\Delta^-)$ and $\alpha_0^-=\alpha_0/(1-i\Delta^+)$. The phase mismatch introduced due to unequal frequencies of pump and probe is given by $\Delta k=k^+-k^-=2(k-k^-)=2(k^+-k)\simeq 2\eta\delta\omega/c$. The complete expressions for all coefficients a_n, b_n, c_n, d_n, and e_n ($n=1,0,-1$) are displayed in Appendix A. Equations (8) are to be solved with the following Fabry-Perot boundary conditions:

$$A_1(0)=rA_2(0)+t_1E_0\,, \tag{10a}$$

$$A_2(L)=rA_1(L)e^{2ikL}\,, \tag{10b}$$

$$A_1^+(0)=rA_2^+(0)\,, \tag{10c}$$

$$A_2^+(L)=rA_1^+(L)e^{2ik^+L}\,, \tag{10d}$$

$$A_1^-(0)=rA_2^-(0)+t_1E_0^-\,, \tag{10e}$$

$$A_2^-(L)=rA_1^-(L)e^{2ik^-L}\,, \tag{10f}$$

where $r=\sqrt{R}$, $t_1=[(1-R)/\eta]^{1/2}$; R is the reflectivity of Fabry-Perot mirrors, E_0 is the incident pump field at frequency ω, and E_0^- is the incident probe at $\omega-\delta\omega$. The Fabry-Perot cavity is located between $z=0$ and $z=L$, as shown in Fig. 1. The reflected and transmitted fields from the Fabry-Perot cavity at three frequencies are given by

$$E_R=rE_0+t_2A_2(0)\,, \tag{11a}$$

$$E_T=t_2A_1(L)e^{ikL}\,, \tag{11b}$$

$$E_R^+=t_2A_2^+(0)\,, \tag{11c}$$

$$E_T^+=t_2A_1^+(L)e^{ik^+L}\,, \tag{11d}$$

$$E_R^-=rE_0^-+t_2A_2^-(0)\,, \tag{11e}$$

$$E_T^-=t_2A_1^-(L)e^{ik^-L}\,, \tag{11f}$$

where $t_2=[\eta(1-R)]^{1/2}$.

IV. MEAN-FIELD APPROXIMATION

In this section, Eqs. (8) are solved under the mean-field approximation by assuming $\alpha_0L\to 0$ and $R\to 1$ with $C_m=\alpha_0L/(1-R)=$constant. This well-known limit corresponds to the experimental case of a high-finesse Fabry-Perot cavity filled with a low-absorption medium. It can be seen that Eqs. (8a) and (8b) for the pump waves do not depend upon the probe and conjugate waves since pump depletion is neglected by assuming $|E^{\pm}(\omega\pm\delta\omega)|\ll|E(\omega)|$. Equations (8a) and (8b) then can be solved separately first. Under the mean-field approximation, fields A_1 and A_2 can be taken independent of z, and hence the right-hand side of Eqs. (8a) and (8b) can be taken as constants. Following the approach developed in Ref. (17), the state equation for the pump is given by

$$I_0=\left|\frac{E_0}{E_s}\right|^2=\eta\frac{(1-R)}{2}I_p\left[\left[1+\frac{C_m}{I_p}(1-s)\right]^2+\left[q-\frac{C_m\Delta}{I_p}(1-s)\right]^2\right], \tag{12}$$

where $I_p=I_1+I_2$, $I_1\approx I_2$, $s=[(1+\Delta^2)/(1+\Delta^2+2I_p)]^{1/2}$, and $q=(2m\pi-2kL)/(1-R)=\theta_1/(1-R)$. Here, m is an integer. The parameter q is a measure of cavity detuning. Mean-field approximation also requires $\theta_1=(2m\pi-2kL)\to 0$. The normalized transmitted intensity I_t can be expressed in terms of I_p by the relation $I_t=1/\eta\,|E_T/E_s|^2=(1-R)I_p/2$.

Now, Eqs. (8c)—(8f) can be solved under the same mean-field approximation since in this case all the fields inside the cavity can be taken independent of z. It may be noticed that for $I_1=I_2$, $b_1=b_{-1}$, $c_1=c_{-1}$, $d_1=d_{-1}$, and $e_1=e_{-1}$ (see Appendix I). The expressions for $A_1^+(L)$ and $[A_1^-(L)]^*$ can be easily obtained after simple but lengthy algebraic calculations as follows:

$$A_1^+(L)=\frac{bt_1(E_0^-)^*}{bc-ad}\,, \tag{13a}$$

and

$$[A_1^-(L)]^*=-\frac{at_1(E_0^-)^*}{bc-ad}\,, \tag{13b}$$

where

$$a=(1-Re^{-i\theta_1}e^{i\Delta kL})+\frac{\alpha_0^+L}{2}[b_0(1+Re^{-i\theta_1}e^{i\Delta kL})+b_1r\nu(e^{-i\theta_1}+1)]\,, \tag{14a}$$

$$b=\frac{\alpha_0^+L}{2}[c_0r\nu(e^{i\theta_1}+1)+c_1(1+Re^{i\theta_1}e^{i\Delta kL})]\,, \tag{14b}$$

$$c=\frac{\alpha_0^-L}{2}[d_0r\nu(e^{-i\theta_1}+1)+d_1(1+Re^{-i\theta_1}e^{i\Delta kL})]\,, \tag{14c}$$

$$d=(1-Re^{i\theta_1}e^{i\Delta kL})+\frac{\alpha_0^-L}{2}[e_0(1+Re^{i\theta_1}e^{i\Delta kL})+e_1r\nu(e^{i\theta_1}+1)]\,, \tag{14d}$$

with $\nu=(e^{i\Delta kL}-1)/i\Delta kL$. The expressions for $A_2^+(0)$ and $[A_2^-(0)]^*$ can be obtained in a quite similar manner. Then, the transmittance coefficients T^+ and T^- for conjugate and probe beams can be written as

$$T^+=\left|\frac{E_T^+}{E_0^-}\right|^2=(1-R)^2\left|\frac{b}{bc-ad}\right|^2, \tag{15a}$$

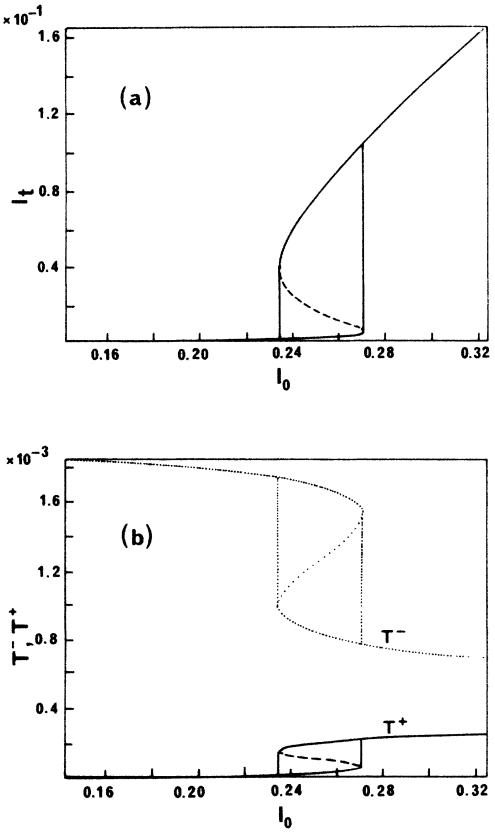

FIG. 2. Showing the bistable behavior of all the three signals (pump, probe, and conjugate) for the case of mean-field approximation. (a) I_t vs I_0 for $\Delta=0$, $q=0$, $\alpha_0 L=0.15$, $R=0.99$, and $\eta=1$. (b) T^- and T^+ vs I_0 for $\Delta kL=0.25$, $\delta\omega T_2=0.5$ and $\delta_1=0.5$. Other parameters in (b) are the same as in (a).

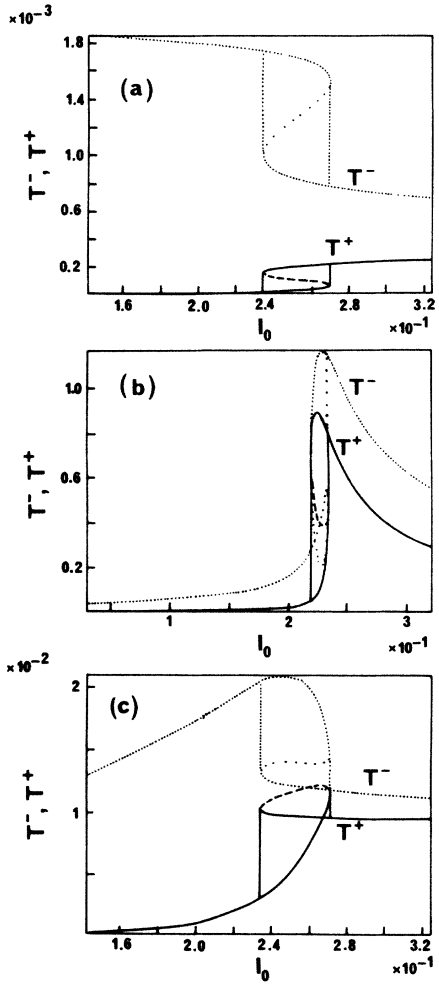

FIG. 3. Plots of T^- and T^+ vs I_0 showing different shapes for probe and conjugate beams. (a) $\Delta=0$; $q=0$, $\alpha_0 L=0.15$, $R=0.99$, $\eta=1$, $\Delta kL=0.25$, $\delta\omega T_2=0.5$, and $\delta_1=0.5$; (b) $\Delta=2$, $q=2$, $\alpha_0 L=0.2$, $R=0.99$, $\eta=1$, $\Delta kL=0.01$, $\delta\omega T_2=0.5$, and $\delta_1=0.5$; (c) $\Delta=0$, $q=0$, $\alpha_0 L=0.15$, $R=0.99$, $\eta=1$, $\Delta kL=0.05$, $\delta\omega T_2=0.7$, and $\delta_1=0.7$.

and

$$T^- = \left| \frac{E_T^-}{E_0^-} \right|^2 = (1-R)^2 \left| \frac{a}{bc-ad} \right|^2 . \tag{15b}$$

Figure 2 shows the behavior of pump, probe, and conjugate signals when the incident driving intensity $I_0 = |E_0/E_s|^2$ is varied in a continuous manner. Figure 2(a) shows the plot of I_t versus I_0 when $q=0$, $\Delta=0$, $\alpha_0 L=0.15$, $R=0.99$, and $\eta=1$, whereas in Fig. 2(b) T^- and T^+ are plotted versus I_0 for $\Delta kL=0.25$, $\delta\omega T_2=0.5$, and $\delta_1=0.5$ with other parameters same as in Fig. 2(a). It can be easily noticed that the turning points of bistability in all the three signals occur at the same values of I_0. As is well known, the pump signal shows bistable behavior because the state equation permits up to three solutions for the intracavity pump intensity for a given set of input parameters where two of these three solutions are stable. The bistability in probe and conjugate signals arises from the dependence of the corresponding nonlinear polarization on the intracavity pump intensity.[12] In this way, a turning point of bistability in the pump signal should also give a turning point in the probe and conjugate signals, occurring at the same input pump intensity. In Fig. 3 some more plots of probe and conjugate transmittance T^- and T^+ are shown for different values of parameters involved. Figure 2(b) is repeated in Fig. 3(a) in order to make a comparison of the different shapes of bistability. The probe transmittance in Fig. 3(a) has a Z type of shape, whereas the conjugate has the usual S-type behavior. In Fig. 3(b) the probe displays a complicated loop, whereas the conjugate shows S-type behavior with the upper stable branch showing a decrease in conjugate transmittance when I_0 is increased. In Fig. 3(c), the probe transmittance shows behavior somewhat similar to the Z type, whereas the conjugate shows a complicated loop, similar to the one obtained by Agrawal (see in Ref. 12).
12).

In Fig. 4 a new phenomenon is explained where a very strong resonance behavior of probe and conjugate transmittance is obtained for certain values of parameters when the pump state equation (12) does not show bistabil-

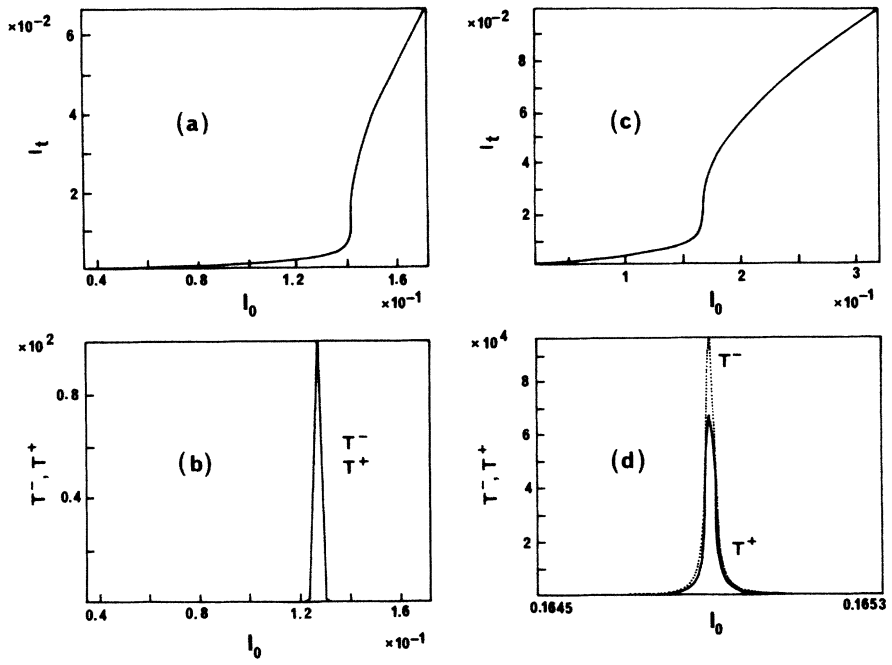

FIG. 4. Illustrating the resonance behavior of probe and conjugate beams with respect to I_0. (a) I_t vs I_0 for $\Delta=0$, $q=0$, $\alpha_0 L=0.1$, $R=0.99$, and $\eta=1$; (b) T^- and T^+ vs I_0 for $\Delta kL=10^{-4}$, $\delta\omega T_2=10^{-4}$, and $\delta_1=10^{-4}$. Other parameters in (b) are the same as in (a). (c) I_t vs I_0 for $\Delta=2$, $q=2$, $\alpha_0 L=0.17$, $R=0.99$, and $\eta=1$; (d) T^- and T^+ vs I_0 for $\Delta kL=10^{-3}$, $\delta\omega T_2=0.5$, and $\delta_1=0.5$. Other parameters in (d) are the same as in (c). Note that the horizontal scale is different in (c) and (d).

ity. For Figs. 4(a) and 4(b) the various parameters are taken as follows: $\Delta=0$, $q=0$, $\alpha_0 L=0.1$, and $R=0.99$. The pump does not show bistability. For $\Delta kL=10^{-4}$, $\delta\omega T_2=10^{-4}$, and $\delta_1=10^{-4}$ the probe and conjugate transmittance curves coincide and they exhibit strong resonance with respect to I_0. Even stronger resonance with extremely small width is obtained in Fig. 4(c) and 4(d), where the parameters are $\Delta=2$, $q=2$, $\alpha_0 L=0.17$, and $R=0.99$. Again, the parameters are such that the pump does not show bistability. For $\Delta kL=10^{-3}$, $\delta\omega T_2=0.5$, and $\delta_1=0.5$ the probe and conjugate exhibit strong resonance with respect to I_0. The probe and conjugate transmittance as high as 10^2 in Fig. 4(b) and 10^4 in Fig. 4(d) show the possibility of achieving high values of T^+ and T^-. The calculations were also performed to obtain this type of resonance behavior when pump shows bistability. It was found that T^+ and T^- exhibit resonance behavior with respect to I_0. However, the width of the resonance is quite large and the height very small compared to that shown in Figs. 4(b) and 4(d). It may be noticed that in Figs. 4(b) and 4(d), ΔkL is very small. This shows that strong resonance with high values of T^+ and T^- may be associated with Fabry-Perot resonance along with the interplay of other parameters. By using these cavity resonances it may be possible to generate intense short-duration pulses at probe and conjugate frequencies even with long-duration input pump pulses. Moreover, comparison of Figs. 4(a) and 4(b) with 4(c) and 4(d) suggests that it could be possible to choose the pulse width by adjusting some of the parameters. Indeed, this pulse width is related to the variation of intracavity pump intensity which strongly depends on the shape of the pump transmittance curve. In Figs. 4(a) and 4(b) the resonance occurs in the region where the transmitted intensity varies quite slowly with the input pump intensity, and the pulse width of probe and conjugate would be large. On the contrary the resonance in Figs. 4(a) and 4(d) occurs for an incident pump intensity corresponding to a rapid increase in the intracavity pump intensity, and the probe and conjugate pulse width would be very narrow. Indeed, probe and conjugate resonances occur for a relative variation in pump intensity smaller than 1%. In this case the pulse width would probably be limited by the cavity or medium response time.

V. SMALL-SIGNAL GAIN APPROXIMATION

In this section Eqs. (8) are solved when α_0 is negative (gain medium) but below laser oscillation threshold (laser amplifier) and for $I_p \ll 1$. Contrary to the absorptive case this low-pump-saturation condition allows for strong nonlinear interactions because as experimentally demonstrated[14] energy transfers are favored by gain. As in the previous case, equations (8a) and (8b) can be solved separately first for forward and backward pump waves A_1 and A_2, and their solutions can be used in solving Eqs. (8c)—(8f). since in this case $I_p \ll 1$, the perturbation method can be used to solve Eq. (8). The susceptibilities χ, χ_1, and χ_4 are now written as

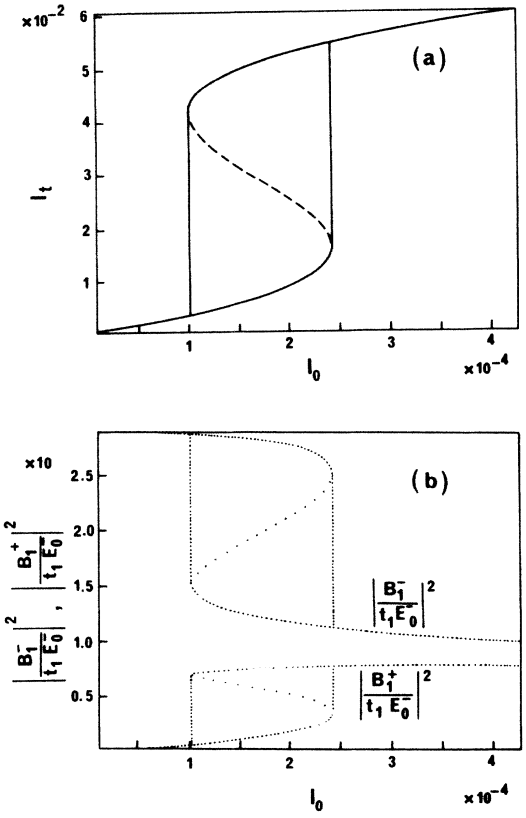

FIG. 5. Showing the bistable behavior of all the three signals (pump, probe, and conjugate) for the case of small-signal gain approximation. (a) I_t vs I_0 for $\Delta=0.1$, $q=0$, $\alpha_0' L=-1.15$, $R=0.3$, and $\eta=3.45$; (b) $|B_1^-/t_1E_0^-|^2$, and $|B_1^+/t_1E_0^-|^2$ vs I_0 for $\Delta kL=0.01$, $\delta\omega T_2=0.05$, and $\delta_1=0.5$. Other parameters in (b) are the same as in (a).

$$\chi=\frac{\alpha_0 c\eta}{4\pi\omega}\frac{\Delta+i}{(1+\Delta^2)^2}\left[1+\Delta^2-\left|\frac{E(\omega)}{E_s}\right|^2\right], \tag{16a}$$

$$\chi_1=\frac{\alpha_0 c\eta}{4\pi\omega}\frac{\Delta^-+i}{1+\Delta^{-2}}\left[1-\left[\frac{1}{1+\Delta^2}-\frac{C^*}{A^*}\right]\left|\frac{E(\omega)}{E_s}\right|^2\right], \tag{16b}$$

$$\chi_4=\frac{\alpha_0 c\eta}{4\pi\omega}\frac{\Delta^+-i}{1+\Delta^{+2}}\left[1-\left[\frac{1}{1+\Delta^2}-\frac{B^*}{A^*}\right]\left|\frac{E(\omega)}{E_s}\right|^2\right], \tag{16c}$$

and χ_2 and χ_3 are still given by Eqs. (4c) and (4d). The quantities A, B, and C in Eqs. (5) now reduce to

$$A=\delta_1-i\ , \tag{17a}$$

$$B=-\frac{1}{2(1+\Delta^2)}\left[\Delta-i-(\Delta^++1)\frac{1+\Delta^2}{1+\Delta^{+2}}\right], \tag{17b}$$

$$C=\frac{1}{2(1+\Delta^2)}\left[\Delta+i-(\Delta^--i)\frac{1+\Delta^2}{1+\Delta^{-2}}\right]. \tag{17c}$$

The solution for the pump equations (8a) and (8b) with the boundary conditions (10a) and (10b) can be expressed in the following form:

$$I_0=A_gI_t-B_gI_t^2+C_gI_t^3\ , \tag{18}$$

where $I_t=(1/\eta)|E_T/E_s|^2$. The coefficients A_g, B_g, and C_g are expressed in Appendix B. Using the same perturbation technique, the solution to equations (8c)–(8f) with the boundary conditions (10c)–(10f) can be written in the following form:

$$\left|\frac{E_T^+}{E_0^-}\right|^2=\eta(1-R)^2\left|e^{-\alpha_0^+L}\right|\left|\frac{B_1^+}{t_1E_0^-}\right|^2, \tag{19a}$$

$$\left|\frac{E_T^-}{E_0^-}\right|^2=\eta(1-R)^2\left|e^{-\alpha_0^-L}\right|\left|\frac{(B_1^-)^*}{t_1E_0^-}\right|^2, \tag{19b}$$

$$\left|\frac{E_R^+}{E_0^-}\right|^2=\eta(1-R)^2\left|e^{-\alpha_0^+L}\right|\left|\frac{B_2'^+}{t_1E_0^-}\right|^2, \tag{19c}$$

$$\left|\frac{E_R^-}{E_0^-}\right|^2=\eta(1-R)^2\left|e^{-\alpha_0^-L}\right|\left|\frac{(B_2'^-)^*}{t_1E_0^-}\right|^2. \tag{19d}$$

In writing Eq. (19d), the term rE_0^- is neglected compared

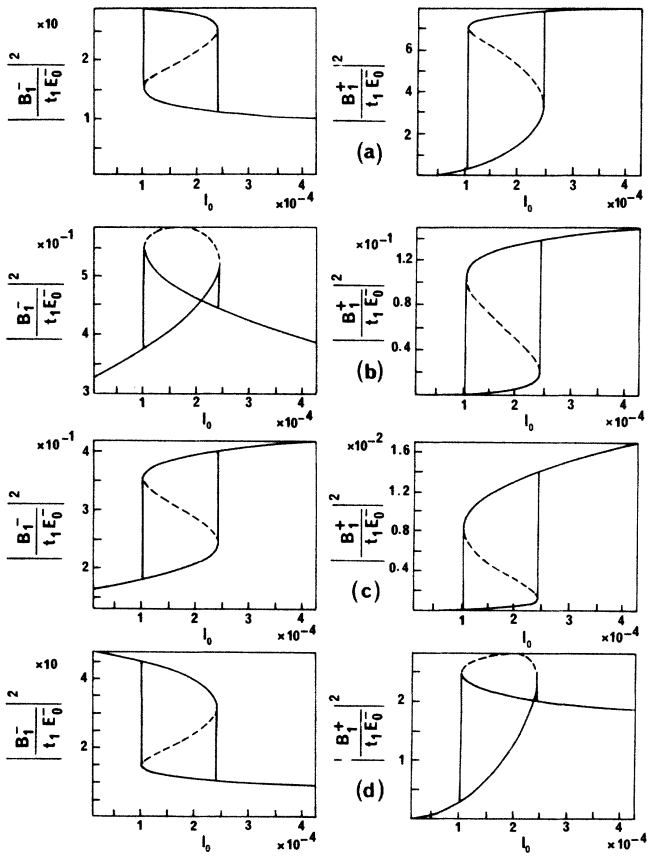

FIG. 6. Plots of $|B_1^-/t_1E_0^-|^2$ and $|B_1^+/t_1E_0^-|^2$ vs I_0 showing different shapes for probe and conjugate beams for the pump parameters as follows: $\Delta=0.1$, $q=0$, $\alpha_0' L=-1.15$, $R=0.3$, and $\eta=3.45$. (a) $\Delta kL=0.01$, $\delta\omega T_2=0.05$, and $\delta_1=0.5$; (b) $\Delta kL=0.25$, $\delta\omega T_2=0.25$, and $\delta_1=0.5$; (c) $\Delta kL=0.5$, $\delta\omega T_2=0.5$, and $\delta_1=0.5$; (d) $\Delta kL=0.01$, $\delta\omega T_2=0.01$, and $\delta_1=0.01$.

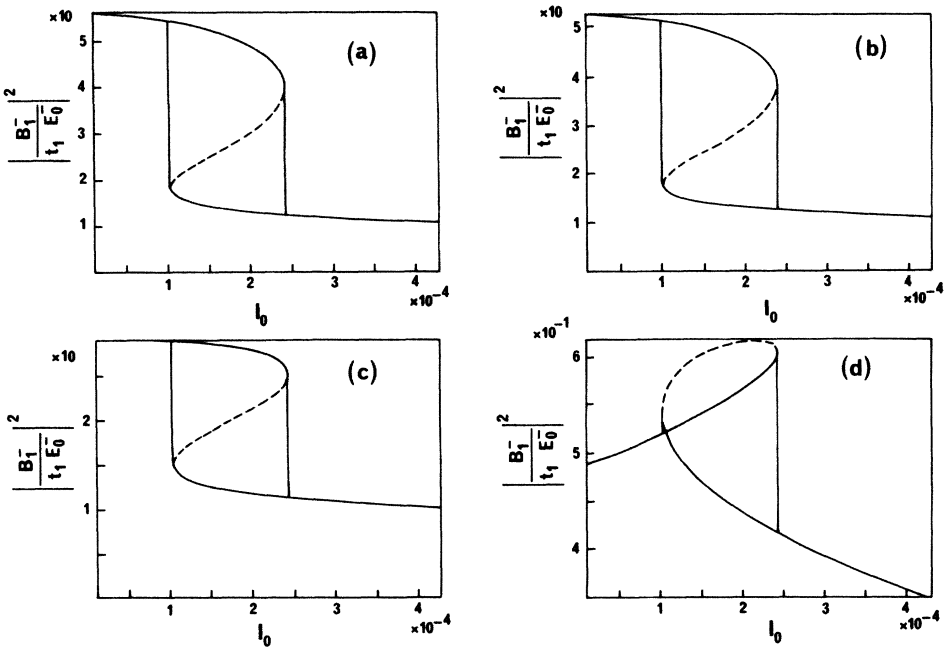

FIG. 7. Plots showing probe amplification dependence on $\delta\omega T_2$. $|B_1^-/t_1E_0^-|^2$ is plotted vs I_0 for $\delta\omega T_2$=(a) 0.0005; (b) 0.005; (c) 0.05; (d) 0.5. Other parameters are $\Delta=0.1$, $q=0$, $\alpha_0'L=-1.15$, $R=0.3$, $\eta=3.45$, $\Delta kL=0.01$, and $\delta_1=0.5$.

to $t_2A_2^-(0)$ in Eq. (11e), assuming that the initial probe is small and that it is substantially amplified inside the cavity. The quantities B_1^+, B_1^-, $B_2'^+$, and $B_2'^-$ appearing in Eqs. (19) satisfy the following four simultaneous linear algebraic equations:

$$\begin{bmatrix} a_{11} & a_{12} & a_{13} & a_{14} \\ a_{21} & a_{22} & a_{23} & a_{24} \\ a_{31} & a_{32} & a_{33} & a_{34} \\ a_{41} & a_{42} & a_{43} & a_{44} \end{bmatrix} \begin{bmatrix} B_1^+/t_1(E_0^-)^* \\ (B_1^-)^*/t_1(E_0^-)^* \\ B_2'^+/t_1(E_0^-)^* \\ (B_2'^-)^*/t_1(E_0^-)^* \end{bmatrix} = \begin{bmatrix} 0 \\ 0 \\ e^{[\alpha_0^- - i(\Delta k+\Delta k_0)]L} \\ re^{[\alpha_0^- - i(\Delta k+\Delta k_0)]L/2} \end{bmatrix} . \quad (20)$$

The coefficients a_{ij} $(i,j=1,2,3,4)$ appearing in Eq. (20) are displayed in Appendix C.

In Fig. 5 the behavior of pump, probe, and conjugate signals is shown when $I_0=|E_0/E_s|^2$ is varied continuously. Figure 5(a) shows the plot of I_t versus I_0 when $\Delta=0.1$, $q=0$, $\eta=3.45$, $R=0.3$, and $\alpha_0'L=\alpha_0L/(1+\Delta^2)=-1.15$. The choice of these parameters corresponds approximately to the operation of laser below about 5% of the threshold for oscillation. In Fig. 5(b) $|B_1^+/t_1E_0^-|^2$ and $|B_1^-/t_1E_0^-|^2$ are plotted versus I_0 for $\Delta kL=0.01$, $\delta\omega T_2=0.05$, and $\delta_1=0.5$. All the three plots show bistable behavior with the turning points in all the three plots occurring at the same values of I_0. It may also be noted that the values of I_0 and I_t in the plots are much less compared to 1. This shows consistency with the assumption $I_p \ll 1$ made in the beginning of this section. In Fig. 6 several other plots are shown for probe and conjugate transmittance for a different set of parameters. All these plots are obtained for the same values of pump parameters ($\Delta=0.1$, $q=0$, $\alpha_0'L=-1.15$, $\eta=3.45$, and $R=0.3$). This figure explains that shapes of bistable behavior of both probe and conjugate beams change for the same shape of bistable behavior of pump beam when ΔkL, $\delta\omega T_2$, and δ_1 are changed. Probe beam has either S-type, Z-type, or a loop-type behavior, whereas the conjugate beam has either S-type or a loop-type shape. In Figs. 7 and 8 the probe and conjugate variations with I_0 for different $\delta\omega T_2$ are shown keeping all the other parameters the same. It can be seen that there is a strong dependence of probe and conjugate amplification on $\delta\omega T_2$ when $\delta\omega T_2$ is less than $\Delta kL/\alpha_0L$. This point is corroborated by the fact that phase conjugation efficiency strongly decreases with large detuning $\delta\omega T_2$.[5] The conjugate amplification saturation occurring at very small normalized detuning $\delta\omega T_2$ is probably due to the cavity detuning $\delta\omega T_2'=\Delta kL/\alpha_0L$ which must be added to $\delta\omega T_2$ when the interaction takes place in a Fabry-Perot cavity.[11] The calculations were also performed by choosing the parameters such that laser operation takes place below but nearer to threshold (2% and 1% below threshold) of oscillation. Larger probe and conjugate amplifications were obtained as laser operated nearer to threshold.

VI. DISCUSSION AND CONCLUSIONS

In this paper theoretical calculations were presented regarding the collinear NDFWM performed inside a nonlinear Fabry-Perot cavity. In this collinear NDFWM pro-

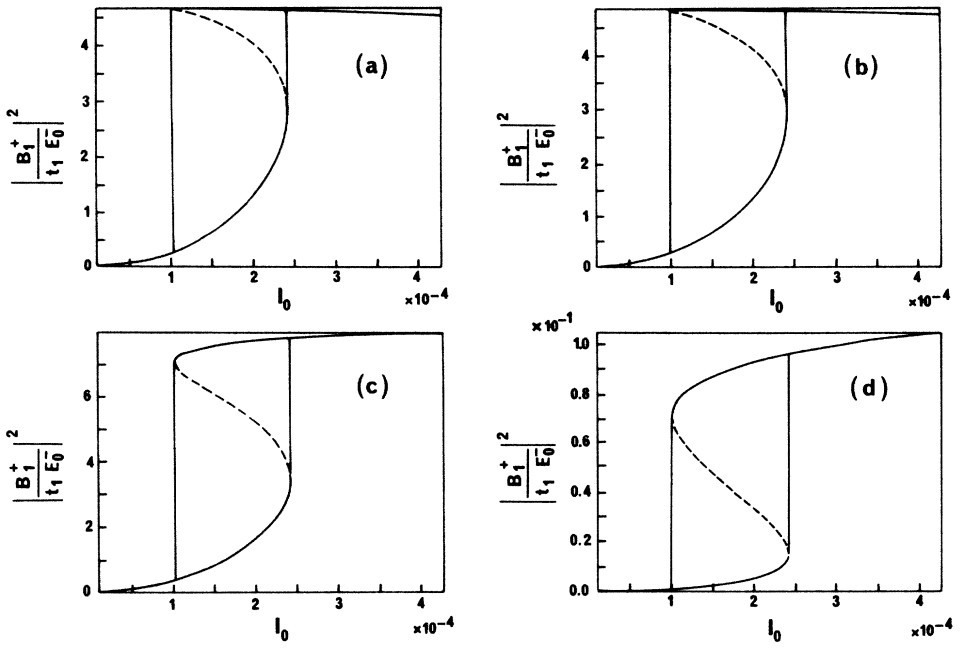

FIG. 8. Plots showing conjugate amplification dependence on $\delta\omega T_2$. $|B_1^+/t_1E_0^-|^2$ is plotted vs I_0 for $\delta\omega T_2$=(a) 0.0005; (b) 0.005; (c) 0.05; (d) 0.5. Other parameters are the same as in Fig. 7. Note that horizontal scale is different in (c) and (d).

cess theoretical calculations are complex since the interaction involves six waves, forward and backward pump, probe, and conjugate, coupled through nonlinearity of the medium. As the interaction occurs inside a Fabry-Perot cavity, each wave is subject to boundary conditions which are interconnected. Therefore, it seems rather difficult to solve the six coupled equations without making any approximations, and hence approximations were applied to simplify the problem. However, the two limits (mean field and small-signal gain) considered in this paper are of considerable interest theoretically as well as experimentally, and hence the results presented in this paper definitely explain some important aspects of collinear intracavity NDFWM process.

The theoretical calculations were carried out assuming that a two-level atomic system was kept inside the Fabry-Perot cavity and that the cavity was externally driven by strong pump beam of frequency ω and probed by a weak beam of frequency $\omega-\delta\omega$. The nonlinear response of the two-level system was calculated using the density matrix formalism and propagation effects were considered by solving coupled wave equations, obtained by substituting nonlinear polarizations at three frequencies of interest into Maxwell's equations, for two different limits mentioned above. The calculations involved a huge amount of algebraic manipulations which were necessary to solve this problem in a Fabry-Perot cavity. Therefore, the numerical computations were also carried out by choosing the common values of the parameters in mean field and small-signal gain approximations to confirm that the calculations did not contain any type of error in both these cases. The common values of the parameters ($\Delta=2$, $q=0$, $\alpha_0 L=-0.04$, $R=0.99$, $\eta=3.45$, $\Delta kL=0.01$, $\delta_1=0.1$, $\delta\omega T_2=0.01$) were chosen in such a way that both the approximations remained valid. Although the bistable behavior in three signals cannot be obtained with the common set of values of the parameters in both the cases, exactly the same plots were obtained for the two limits thus confirming that theoretical calculations presented in this paper contained no error.

The results obtained in each approximation suggest the bistable behavior for all the three signals which, of course is already observed experimentally.[14] Moreover, the calculations suggest that several different shapes of the hysteresis loops can be possible depending upon the system parameters. Some of these shapes are similar to that obtained by Agrawal and Flytzanis, and Agrawal in Ref. 12, although their calculations were performed for the noncollinear intracavity DFWM process using the mean-field approximation. Moreover, it should be recalled that, due to the direct dependence of their intensities on the pump intensity inside the Fabry-Perot cavity, probe and conjugate exhibit bistability at exactly the same input pump intensity as for pump bistability.

In the mean-field approximation, the results of present work also demonstrate a possibility of an experimental observation of a new phenomenon, viz., a very strong resonance behavior of probe and conjugate transmittance with respect to the incident pump intensity in the case when pump does not exhibit bistability. As discussed at the end of Sec. IV, this type of cavity resonances may be utilized to generate intense short-duration pulses at probe and con-

jugate frequencies even when the pump pulses are of long duration. However, it should be mentioned that the present analysis considers the steady-state solutions of the atomic and field variables. Therefore, in order to obtain quantitative information regarding the generation of short-duration pulses at probe and conjugate frequencies, the dynamic aspects of the problem should be considered. This dynamic behavior involves the relaxation time of the nonlinear absorber and the lifetime of photons inside the Fabry-Perot cavity. Therefore, if short duration pulses are desired, the nonlinear medium should have a strong absorption coefficient and short-duration response time. Indeed, in this case the Fabry-Perot cavity should be thin and sufficiently absorptive to give the fast nonlinear response necessary for this kind of operation. With such a setup it could be possible to generate high peak power pulses of variable short duration only by adjusting the pump-medium or pump-cavity detuning. The experiments to obtain these compressed pulses at probe or conjugate frequency could be performed by using thin Fabry-Perot cavities constructed from quantum well structures or composite materials.

The calculations performed by applying the small-signal gain approximation show several interesting results: bistable behavior in all the three signals, very large values of reflected and transmitted conjugate signals obtained with very low input powers, and increase in contrast of bistable probe and conjugate signals compared to pump bistability. These theoretical conclusions are corroborated by the experimental observations of Nakajima and Frey.[14] However, care should be taken while making the direct comparison of the experimental results of Ref. 14 with the analysis presented in this paper for the small-signal gain limit, as the experiments were performed using a semiconductor laser amplifier which is not precisely a homogeneous broadened two-level system. In this case indeed amplifying transitions occur between conduction and valence bands. Even then the theoretical calculations do explain qualitatively all the features of the experimental results. From an experimental point of view, these amplifying setups could be more interesting than passive devices since it could be possible to get very high conjugated reflectivities with low-power input beams. This point has already been confirmed by both calculations and experiments performed when the amplifying Fabry-Perot cavity operates above threshold.[8,11] In the case of bistability it means that practical setups could be built in order to obtain high-contrast logic devices and high-gain differential amplifiers.

Let us stress in a final statement that as the probe and conjugate intensities are directly connected to the pump intensity inside the Fabry-Perot laser cavity the nearly degenerate four-wave mixing technique may be useful for the observation of any instability occurring inside a Fabry-Perot laser cavity.

APPENDIX A

In this appendix, all the coefficients appearing in Eq. (8) are displayed as follows:

$$a_0=[(1+\Delta^2+I_p)^2-4I_1I_2]^{-1/2}, \tag{A1}$$

$$a_1=a_{-1}=\tfrac{1}{2}(I_1I_2)^{-1/2}[1-a_0(1+\Delta^2+I_p)], \tag{A2}$$

$$b_0=\left[\frac{1+\Delta^2}{A_0}\right]+B_0(G+H), \tag{A3}$$

$$b_1=b_{-1}=\left[\frac{1+\Delta^2}{F}\right]\left[1-\frac{E}{A_0}\right]+B_0\left[\frac{I_p}{F}H+J\right], \tag{A4}$$

$$d_0=B_0\left[\frac{I_p}{F}H+\frac{F}{I_p}G\right]e^{-i(q_1+q_2)} \tag{A5}$$

$$d_1=B_0\left[\left[\frac{I_1}{I_2}\right]^{1/2}J-\frac{(I_1-I_2)}{I_P}G+H\right]e^{-i(q_1+q_2)}, \tag{A6}$$

$$d_{-1}=B_0\left[\left[\frac{I_2}{I_1}\right]^{1/2}J+\frac{(I_1-I_2)}{I_p}G+H\right]e^{-i(q_1+q_2)}, \tag{A7}$$

$$c_0=B_1\left[\frac{I_p}{F}H+\frac{F}{I_p}G\right]e^{i(q_1+q_2)}, \tag{A8}$$

$$c_1=B_1\left[\left[\frac{I_2}{I_1}\right]^{1/2}J+\frac{(I_1-I_2)}{I_p}G+H\right]e^{i(q_1+q_2)}, \tag{A9}$$

$$c_{-1}=B_1\left[\left[\frac{I_1}{I_2}\right]^{1/2}J-\frac{(I_1-I_2)}{I_p}G+H\right]e^{i(q_1+q_2)}, \tag{A10}$$

$$e_0=\left[\frac{1+\Delta^2}{A_0}\right]+B_1(G+H), \tag{A11}$$

$$e_1=e_{-1}=\left[\frac{1+\Delta^2}{F}\right]\left[1-\frac{E}{A_0}\right]+B_1\left[\frac{I_p}{F}H+J\right], \tag{A12}$$

where

$$I_p=I_1+I_2,$$

$$A_0=a_0^{-1},$$

$$B_0=\frac{1}{2}\left[\Delta-i-(\Delta^-+i)\frac{1+\Delta^2}{1+\Delta^{-2}}\right],$$

$$B_1=-\frac{1}{2}\left[\Delta+i-(\Delta^+-i)\frac{1+\Delta^2}{1+\Delta^{+2}}\right],$$

$$C_0=\delta_1+i+\frac{1}{2}\left[\frac{\Delta^-+i}{1+\Delta^{-2}}-\frac{\Delta^+-i}{1+\Delta^{+2}}\right]I_p,$$

$$D=(I_1I_2)^{1/2}\left[\frac{\Delta^-+i}{1+\Delta^{-2}}-\frac{\Delta^+-i}{1+\Delta^{+2}}\right],$$

$$E=1+\Delta^2+I_p,$$

$$F=2(I_1I_2)^{1/2},$$

$$G=\frac{I_p}{FC_0-ED}\left[\frac{F}{A}-D(C_0^2-D^2)^{-1/2}\right],$$

$$H=-\frac{F}{FC_0-ED}\left[\frac{E}{A}-C_0(C_0^2-D^2)^{-1/2}\right],$$

$$J=D^{-1}+F(FC_0-ED)^{-1}\left[\frac{E^2}{FA}-\frac{C_0^2}{D}(C_0^2-D^2)^{-1/2}\right].$$

APPENDIX B

In this appendix, the coefficients A_g, B_g, and C_g appearing in Eq. (18) are displayed as follows:

$$A_g=\frac{\eta\,|e'|^2}{(1-R)^2}e^{\alpha_0' L}\,, \tag{B1}$$

$$B_g=\frac{\eta}{(1-R)^3}e^{2\alpha_0' L}(e'^{*}a'b'+e'a'^{*}b'^{*})\,, \tag{B2}$$

$$C_g=\frac{\eta\,|a'|^2}{(1-R)^4}e^{3\alpha_0' L}\,, \tag{B3}$$

where

$$\alpha_0'=\frac{\alpha_0}{1+\Delta^2}\,,$$

$$\Delta k_0=\frac{\alpha_0\Delta}{1+\Delta^2}\,,$$

$$q'=\frac{\alpha_0 L\,\Delta}{1+\Delta^2}-\theta_1\,,$$

$$\theta_1=2m\pi-2kL\,,$$

$$e'=1-Re^{-\alpha_0' L}e^{iq'}-i\Psi\,,$$

$$b'=\frac{[1-2R(\cos q')e^{-\alpha_0' L}+R^2e^{-2\alpha_0' L}]}{(1-Re^{-\alpha_0' L}e^{iq'})^2}\,,$$

$$\Psi=\frac{b'}{1-R}e^{iq'}I_t e^{-\alpha_0' L}(1+Re^{2iq'})\frac{3R\sin(\Delta k_0 L)}{2(1+\Delta^2)}\,,$$

$$\Psi_1=(1-e^{-\alpha_0' L}e^{i\Delta k_0 L})\left[e^{\alpha_0' L}+\frac{R}{2}e^{2iq'}e^{-i\Delta k_0 L}\right],$$

$$\Psi_2=1-Re^{-2\alpha_0' L}e^{i\Delta k_0 L}e^{iq'}\,,$$

$$\Psi_3=e^{-2\alpha_0' L}e^{2iq'}(Re^{-i\Delta k_0 L}e^{iq'}-1)\,,$$

$$a'=\frac{R}{1+\Delta^2}e^{-2\alpha_0' L}e^{iq'}\Psi_1+\frac{1}{2(1+\Delta^2)}\Psi_2+\frac{R}{(1+\Delta^2)}\Psi_3.$$

APPENDIX C

In this appendix, the coefficients a_{ij} appearing in Eq. (20) are displayed as follows:

$$a_{11}=RB_p(e^{(\alpha_0^{+}-i\Delta k)L}-e^{-i\Delta k_0 L})-A_p[R(1-R)+(Re^{-\alpha_0' L}-e^{\alpha_0' L})e^{(\alpha_0^{+}-i\Delta k)L}]-\mu_1\,, \tag{C1}$$

$$a_{12}=-[B_p(1-Re^{i\Delta k_0 L})+A_p(1-R+Re^{-\alpha_0' L}-e^{\alpha_0' L})]re^{(\alpha_0^{+}-i\Delta k)L/2}\,, \tag{C2}$$

$$a_{13}=[RD_p(1-e^{-(\alpha_2-i\Delta k)L})-C_p e^{\alpha_0' L}(1-Re^{-\alpha_0' L}e^{-[\alpha_2-i(\Delta k+\Delta k_0)]L})]e^{(\alpha_0^{+}-i\Delta k)L}\,, \tag{C3}$$

$$a_{14}=[RC_p e^{-\alpha_0' L}(e^{\alpha_3 L}-e^{(\alpha_0'-i\Delta k_0)L})-D_p(e^{\alpha_3 L}-R)]re^{(\alpha_0^{+}-i\Delta k)L/2}\,, \tag{C4}$$

$$a_{21}=-[A_p(1-R+Re^{-\alpha_0' L}-e^{\alpha_0' L})+B_p(e^{-i\Delta k_0 L}-R)]re^{(\alpha_0^{+}-i\Delta k)L/2}\,, \tag{C5}$$

$$a_{22}=RB_p(e^{[\alpha_0^{+}-i(\Delta k-\Delta k_0)]L}-1)-A_p[R(Re^{-\alpha_0' L}-e^{\alpha_0' L})+(1-R)e^{(\alpha_0^{+}-i\Delta k)L}]-\mu_1\,, \tag{C6}$$

$$a_{23}=[C_p(e^{(\alpha_3+i\Delta k_0)L}-e^{\alpha_0' L})-D_p(e^{\alpha_3 L}-R)]re^{(\alpha_0^{+}-i\Delta k)L/2}\,, \tag{C7}$$

$$a_{24}=[D_p(1-e^{-(\alpha_2-i\Delta k)L})-C_p(e^{-i\Delta k_0 L}-Re^{-\alpha_0' L}e^{-(\alpha_2-i\Delta k)L})]Re^{(\alpha_0^{+}-i\Delta k)L}\,, \tag{C8}$$

$$a_{31}=[RD_p'(1-e^{-(\alpha_2-i\Delta k)L})-C_p'(e^{\alpha_0' L}-Re^{-[\alpha_2-i(\Delta k-\Delta k_0)]L})]e^{(\alpha_0^{-}-i\Delta k)L}\,, \tag{C9}$$

$$a_{32}=[RC_p'e^{-\alpha_0' L}(e^{-\alpha_3 L}-e^{(\alpha_0'+i\Delta k_0)L})-D_p'(e^{-\alpha_3 L}-R)]re^{(\alpha_0^{-}-i\Delta k)L/2}\,, \tag{C10}$$

$$a_{33}=RB_p'(e^{(\alpha_0^{-}-i\Delta k)L}-e^{i\Delta k_0 L})-A_p'[R(1-R)+(Re^{-\alpha_0' L}-e^{\alpha_0' L})e^{(\alpha_0^{-}-i\Delta k)L}]-\mu_2\,, \tag{C11}$$

$$a_{34}=-[A_p'(1-R+Re^{-\alpha_0' L}-e^{\alpha_0' L})+B_p'(1-Re^{-i\Delta k_0 L})]re^{(\alpha_0^- -i\Delta k)L/2}, \tag{C12}$$

$$a_{41}=[C_p'(e^{-(\alpha_3+i\Delta k_0)L}-e^{\alpha_0' L})-D_p'(e^{-\alpha_3 L}-R)]re^{(\alpha_0^- -i\Delta k)L/2}, \tag{C13}$$

$$a_{42}=[C_p'(Re^{-\alpha_0' L}e^{-(\alpha_2-i\Delta k)L}-e^{i\Delta k_0 L})-D_p'(e^{-(\alpha_2-i\Delta k)L}-1)]\mathrm{Re}^{(\alpha_0^- -i\Delta k)L}, \tag{C14}$$

$$a_{43}=-[B_p'(e^{i\Delta k_0 L}-R)+A_p'(1-R+Re^{-\alpha_0' L}-e^{\alpha_0' L})]re^{(\alpha_0^- -i\Delta k)L/2}, \tag{C15}$$

$$a_{44}=RB_p'(e^{[\alpha_0^- -i(\Delta k+\Delta k_0)]L}-1)-A_p'[R(Re^{-\alpha_0' L}-e^{\alpha_0' L})+(1-R)e^{(\alpha_0^- -i\Delta k)L}]-\mu_2, \tag{C16}$$

where

$$A_p=-\frac{I_t}{2(1-R)}\beta^+\frac{\alpha_0^+}{\alpha_0'},$$

$$B_p=-\frac{I_t}{2(1-R)}\beta^+\frac{\alpha_0^+}{\alpha_0^+-i(\Delta k-\Delta k_0)},$$

$$C_p=\frac{I_t}{2(1-R)}\gamma^+\frac{\alpha_0^+}{\alpha_1-i\Delta k_0},$$

$$D_P=-\frac{I_t}{(1-R)}\gamma^+\frac{\alpha_0^+}{\alpha_2-i\Delta k},$$

$$A_p'=-\frac{I_t}{2(1-R)}\beta^-\frac{\alpha_0^-}{\alpha_0'},$$

$$B_p'=-\frac{I_t}{2(1-R)}\beta^-\frac{\alpha_0^-}{\alpha_0^- -i(\Delta k+\Delta k_0)},$$

$$C_p'=\frac{I_t}{2(1-R)}\gamma^-\frac{\alpha_0^-}{\alpha_1'+i\Delta k_0},$$

$$D_p'=-\frac{I_t}{(1-R)}\gamma^-\frac{\alpha_0^-}{\alpha_2-i\Delta k},$$

$$\mu_1=e^{(\alpha_0^+ -i\Delta k)L}-R,$$

$$\mu_2=e^{(\alpha_0^- -i\Delta k)L}-R,$$

$$\beta^+=\frac{C^*}{A^*}-\frac{1}{1+\Delta^2},\quad \beta^-=\frac{B^*}{A^*}-\frac{1}{1+\Delta^2},$$

$$\gamma^+=B^*/A^*,\quad \gamma^-=C^*/A^*,$$

$$\alpha_0'=\alpha_0/(1+\Delta^2),$$

$$\alpha_1=\alpha_0'-\tfrac{1}{2}(\alpha_0^+-\alpha_0^-),$$

$$\alpha_2=\tfrac{1}{2}(\alpha_0^++\alpha_0^-),$$

$$\alpha_3=\tfrac{1}{2}(\alpha_0^+-\alpha_0^-),$$

and

$$\alpha_1'=\alpha_0'+\alpha_3.$$

[1]H. M. Gibbs, S. L. McCall, and T. N. C. Venkatesan, Phys. Rev. Lett. **35**, 1135 (1976).

[2]R. W. Hellwarth, J. Opt. Soc. Am. **67**, 1 (1977).

[3]K. Ikeda, H. Daido, and O. Akimoto, Phys. Rev. Lett. **45**, 709 (1980).

[4]A. Yariv, IEEE J. Quant. Electron. **QE-14**, 650 (1978); J. P. Huignard, J. P. Herriau, P. Aubourg, and E. Spitz, Opt. Lett. **4**, 21 (1979); A. Yariv, in *Physics of Quantum Electronics*, edited by S. F. Jacobs, M. Sargent III, and M. O. Scully (Addison-Wesley, Reading, Mass., 1978), Vol. 6, p. 175; J. AuYoung, D. Fekete, D. M. Pepper, and A. Yariv, IEEE J. Quant. Electron. **QE-15**, 1180 (1979); P. A. Belanger, A. Hardy, and A. E. Siegman, Appl. Opt. **19**, 602 (1980); J. F. Lam and W. P. Brown, Opt. Lett. **5**, 61 (1980).

[5]D. M. Pepper and R. L. Abrams, Opt. Lett. **3**, 212 (1978); J. Nilsen and A. Yariv, Appl. Opt. **18**, 143 (1979); Opt. Commun. **39**, 199 (1981); IEEE J. Quant. Electron. **QE-18**, 1947 (1982); D. J. Harter and R. W. Boyd, IEEE J. Quant. Electron. **QE-16**, 1126 (1980); J. Nilsen, N. S. Gluck, and A. Yariv, Opt. Lett. **6**, 380 (1981); D. G. Steel and R. C. Lind, Opt. Lett. **6**, 587 (1981); F. Tao-Yi and M. Sargent III, Opt. Lett. **4**, 366 (1979); J. Nilsen and A. Yariv, J. Opt. Soc. Am. **71**, 180 (1981).

[6]R. L. Abrams and R. C. Lind, Opt. Lett. **2**, 94 (1978); Opt. Lett. **3**, 205 (1978); P. F. Liao, D. M. Bloom, and N. P. Economous, Appl. Phys. Lett. **32**, 813 (1978); D. M. Bloom, P. F. Liao, and N. P. Economous, Opt. Lett. **2**, 58 (1978); E. I. Moses and F. Y. Wu, Opt. Lett. **5**, 64 (1980); D. G. Steel, R. C. Lind, and F. J. Lam, Phys. Rev. A **23**, 2513 (1981); D. M. Bloom and G. C. Bjorklund, Appl. Phys. Lett. **31**, 592 (1977); G. J. Dunning and D. G. Steel, IEEE J. Quant. Electron. **QE-18**, 3 (1982).

[7]J. Reintjes and L. J. Palumbo, IEEE J. Quant. Electron. **QE-18**, 1934 (1982); A. Tomita, Appl. Phys. Lett. **34**, 463 (1979); R. A. Fisher and B. J. Feldman, Opt. Lett. **4**, 140 (1979); E. E. Bergmann, I. J. Bigio, B. J. Feldman, and R. A. Fisher, Opt. Lett. **3**, 82 (1978).

[8]H. Nakajima and R. Frey, Appl. Phys. Lett. **47**, 769 (1985).

[9]M. Ducloy and D. Bloch, J. Phys. Paris **42**, 711 (1981); R. K. Raj, D. Bloch, J. J. Snyder, G. Camy, and M. Ducloy, Phys. Rev. Lett. **44**, 1251 (1980).

[10]J. H. Marburger and J. F. Lam, Appl. Phys. Lett. **34**, 389 (1979); Appl. Phys. Lett. **35**, 249 (1979); D. K. Saldin, T. Wilson, and L. Solymar, J. Opt. Soc. Am. **72**, 1179 (1982).

[11]R. Frey, Opt. Lett. **11**, 91 (1986).
[12]G. P. Agrawal and C. Flytzanis, IEEE J. Quant. Electron. **QE-17**, 374 (1981); G. P. Agrawal, C. Flytzanis, R. Frey, and F. Pradère, Appl. Phys. Lett. **38**, 492 (1981); L. Fu-Li, J. A. Hermann and J. N. Elgin, Opt. Commun. **40**, 446 (1982); G. P. Agrawal, J. Opt. Soc. Am. **73**, 654 (1983).
[13]E. Köster, J. Kolbe, F. Mitschke, J. Mlynek, and W. Lange, Appl. Phys. B **35**, 201 (1984).
[14]H. Nakajima and R. Frey, Phys. Rev. Lett. **54**, 1798 (1985).
[15]N. Bloembergen and Y. R. Shen, Phys. Rev. **133**, A37 (1964).
[16]See, for example, the papers of J. Nilsen and A. Yariv, and D. J. Harter and R. W. Boyd in Ref. 5.
[17]G. P. Agrawal and H. J. Carmichael, Opt. Acta **27**, 651 (1980).